On the Investigation of the Structure of Amorphous Substances by Means of Electron Diffraction

Frieder Paasche, Herbert Olbrich, Ute Schestag, Peter Lamparter, and Siegfried Steeb
Max-Planck-Institut für Metallforschung, Institut für Werkstoffwissenschaften, Stuttgart

Z. Naturforsch. **37a**, 1139–1146 (1982); received May 3, 1982

A "Scanning High Energy Electron Diffraction"-(SHEED-)apparatus is described with which the intensity curves of elastically scattered electrons are obtained within a few minutes. The elimination of the inelastic background is done by means of an electrostatic filter with an energy resolution of 10^4, which is only limited by the line width of the beam producing system. The intensity curves obtained experimentally are corrected for multiple scattering.

The pair correlation functions of amorphous Germanium as obtained by electron and X-ray diffraction are compared. The electron diffraction curves agree well with the corresponding curves of other authors. The same stands for the curves obtained with X-rays. The differences between the curves obtained with electrons and X-rays are discussed.

Introduction

Electrons are, besides X-rays and neutrons, another qualified probe for the investigation of atomic structures. For performing reliable diffraction experiments, so called SHEED-apparatus (Scanning High Energy Electron Diffraction) with energy filter are in use since several years (see e. g. [1–3]). In the following the SHEED-apparatus used in the present study is described. An electrostatic filter allows the direct registration of the elastically scattered intensity.

In order not to be limited to extremely thin specimens, a correction method for multiple scattering is applied, which is checked using amorphous Germanium films obtained by high vacuum evaporation technique with different thicknesses.

Theoretical Background

The structural information obtained for example by scattering of electrons with amorphous elements, is primarily given by the structure factor $S(Q)$, which is calculated from the normalized coherently scattered intensity I_{coh} according to

$$S(Q) = I_{\mathrm{coh}}(Q)/a f^2(Q) \qquad (1)$$

with $Q = 4\pi(\sin\theta)/\lambda$, θ = half of the scattering angle, λ = wavelength, a = normalizing constant, $f(Q)$ = scattering length of the concerning kind of atoms for electrons.

From $S(Q)$, the pair correlation function $G(r)$ for the case of spherical symmetry is obtained by the equation

$$G(r) = 4\pi r[\varrho(r) - \varrho_0] = \frac{2}{\pi}\int_0^\infty Q[S(Q) - 1]\sin(Q r)\,\mathrm{d}Q \qquad (2)$$

with r = coordinate in real space, ϱ = local atomic number density, ϱ_0 = average atomic number density.

The atomic distribution function

$$A(r) = 4\pi r^2 \varrho(r) = 4\pi r^2 \varrho_0 + r\,G(r) \qquad (3)$$

represents the number of atoms per unit thickness in a spherical shell with the radius r.

Construction and Properties of the Apparatus

The electron diffraction apparatus is used for quantitative detection of radial symmetric electron diffraction patterns of polycrystalline or amorphous specimens. The diffraction pattern is scanned over an aperture which defines the resolution (defining aperture). An electrostatic energy filter eliminates the inelastically scattered electrons. The recording is done by a surface barrier-detector. The whole diffraction diagram is stored in a multi-channel-analyzer and can be read into a computer for further calculation. Figure 1 shows the apparatus schematically.

Reprint requests to Prof. Dr. S. Steeb, Max-Planck-Institut für Metallforschung, Institut für Werkstoffwissenschaften, Seestrasse 92, D-7000 Stuttgart 1.

0340-4811 / 82 / 1000-1139 $ 01.30/0. — Please order a reprint rather than making your own copy.

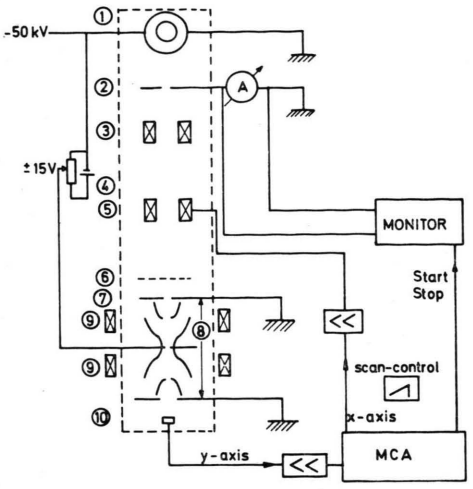

Fig. 1. Schematic Diagram of the SHEED-apparatus;
1 Iduni-cathode
2 Anode diaphragm
3 Condensor
4 Specimen holder
5 Scanning coil
6 Fluorescent screen
7 Aperture diaphragm
8 Electrostatic energy filter
9 Correction coils
10 Semiconductor-Detector

The beam source is an Iduni-cathode [4], which works with 50 kV and so provides electrons with a wavelength of about 0.05 Å. It should be mentioned that the detected Q-region up to 15 $Å^{-1}$ corresponds to a diffraction angle of $2\theta \approx 7°$. The Iduni-cathode has the advantage that it works nearly without servicing and provides a rather large beam intensity which causes short measuring times. On the other hand two disadvantages should be mentioned: The directional beam value is about two powers of magnitude smaller than with the hairneedle-cathode [4]. However, this point is not important for electron diffraction work. Furthermore the energy distribution of the generated electrons is four times as broad as with the hairneedle-cathode.

To obtain absolutely comparable results a monitor for the electron-current is used. The voltage at the current measuring instrument (Fig. 1) is transferred into a voltage-proportional frequency, the periods of which are counted. That means a temporal integration over the beam current. This integral forms a relative measure for the total number of electrons passing the specimen during the measuring time. Thus the measurement can be normalized and the intensities obtained can be compared directly with each other.

The process of scanning is driven by the multichannel-analyzer using the multi-channel-scaling-option. Hereby the MCA counts for a defined time into the first channel, then into the second channel and so on. The scan process is directed by a voltage which is produced by the MCA and which is proportional to the present channel number. This voltage is applied to a power-amplifier which supplies the scanning coil. The proportional-factor and a constant shift can be preselected at the amplifier. Thus to each channel number belongs a certain deviation of the diffraction pattern and at the same time a certain diffraction angle in which the electrons just reach the aperture diaphragm. As a scanning coil the coil of a SEM (JXA-50A, Jeol, Tokyo) was used.

The electrostatic filter produces a potential hill of 50 keV which can only be passed by those electrons which are scattered elastically. Looking at position 8 in Fig. 1, the curved part in the middle is the cathode. From the top and from the bottom the two anodes tower in, which lie on ground potential. The anode beneath the cathode accelerates those electrons which have passed the potential hill to 50 keV. So they can be detected with the detector. A description of the filter is given in [5].

The connection of the filter to the high voltage power supply is shown in Figure 2. The filter is connected in parallel to the electron source. So both parts follow eventual drifts in the same manner and therefore these have no influence on the energy-resolution [6]. The main feature of the present electrostatic filter is the exact cut-off beneath a defined energy and at the same time a good trans-

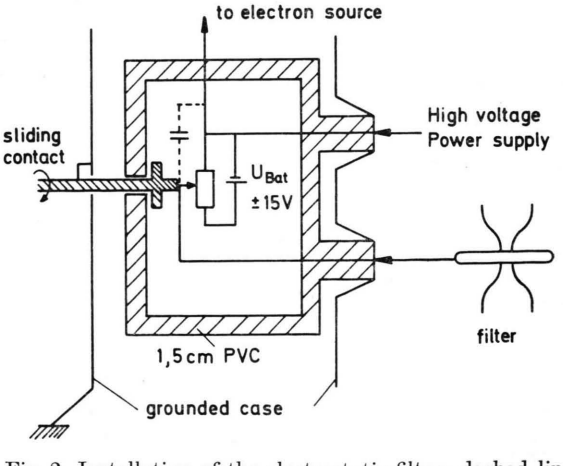

Fig. 2. Installation of the electrostatic filter; dashed line: Over voltage conductor for the protection of the potentiometer.

parency for all energies lying above. With the filter used, the energy resolution is better than 0.5 eV.

Corresponding to [7] the deviation of the energy level is smaller than 0.1 eV during a decalibration of 2 mm out of the optical axis. By placing the scanning coil directly beneath the specimen it could be reached that the maximum angle under which the electron beam passes the filter amounts to 0.81°, which means a deviation of 4 mm directly above the detector. If one assumes a quadratic dependence from the angle [6], this corresponds to 0.4 eV. This is a value which cannot be reached by ring electrodes with simple (circular) profiles. Merely a conic profile of the ring electrodes provides much better properties. By using an aperture diaphragm (detector surface) as large as possible beneath the filter, the second condition, namely that all electrons above the level pass the filter, is fulfilled [8]. With the smallest used detector (active surface 12 mm^2) the whole angle region could be recorded. This shows an additional focussing effect of the filter. By using a larger detector (50 mm^2) the condition is certainly accomplished. An even larger detector (100 mm^2) is used for measuring with switched off filter.

By reducing the energy level a defocussing of the electron beam occurs which can be corrected by an axial magnetic field. Therefore, Helmholtz-coils were installed around the filter outside the vacuum [9]. The needed coil-current at different levels was found by watching the primary beam on a fluorescent-screen beneath the filter.

For registration of the electrons a surface-barrier detector (Canberra, Frankfurt/Main) with a depletion depth of 100 µ was used. The mass per unit area of the deposited gold-contact which the electrons have to pass amounts to 40 $\mu g/cm^2$. The registration-electronic is layed out for 70 kcps. The data were read into a multi-user computer PDP11/34. To measure the diffracted intensities of a polycrystalline gold-film with different resolution, aperture-diaphragmas of 200 µm, 400 µm, and 1000 µm were used. The corresponding half-widths were 0.154 $Å^{-1}$, 0.190 $Å^{-1}$, and 0.322 $Å^{-1}$. To obtain sufficient intensity, the present diffraction experiments were performed using a 400 µm diaphragm. The proportionality between the channel-position of the peak in the MCA and the corresponding value of $Q = 4\pi(\sin\theta/\lambda)$ (θ = half of the diffraction angle; λ = wavelength of the electrons) was also verified by measurements with polycrystalline gold-films.

Measurements

In this section first of all we will discuss to what degree inelastic scattering effects can be eliminated with the apparatus described. Furthermore the influence of multiple scattering shall be investigated using amorphous Germanium-films with different thicknesses. Regarding all these effect we finally will arrive at the intensity curve of the coherently single scattered electrons.

The energy distribution of the electrons in the primary beam was determined by measuring the intensity of the primary beam for different potential walls of the filter (U_{Bat} in Figure 2). By forming the first derivative of these curves one obtains energy spectra as given in Figure 3 [6].

The energy spectrum of amorphous $Mn_{73}Si_{27}$ (see curve d in Fig. 3) deviates in the region between 1 and 4 Volt from the curves b) and c) which represent the "normal" behaviour [4]. The line width of the energy distribution of the primary electrons amounts 4 to 5 eV. The maxima in the spectra of Germanium and of $Mn_{73}Si_{27}$ at about -7 eV are ascribed to inelastic scattering connected with plasmon excitations [6, 10]. Thus we recognize

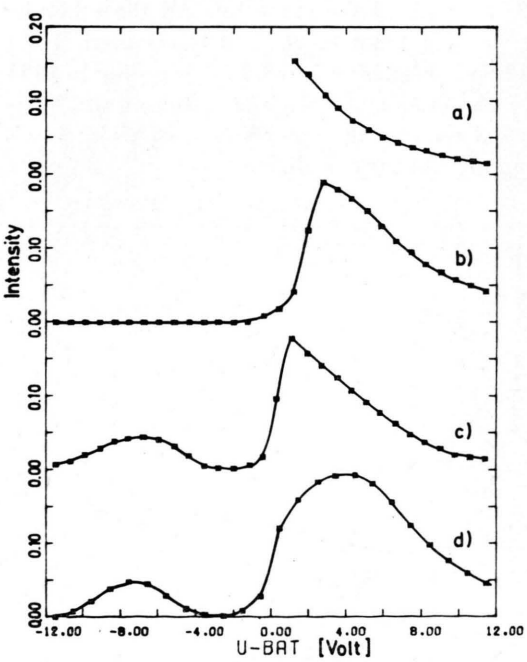

Fig. 3. Energy distribution of the primary beam;
a) Without specimen c) Germanium
b) Gold d) Manganese-Silicone

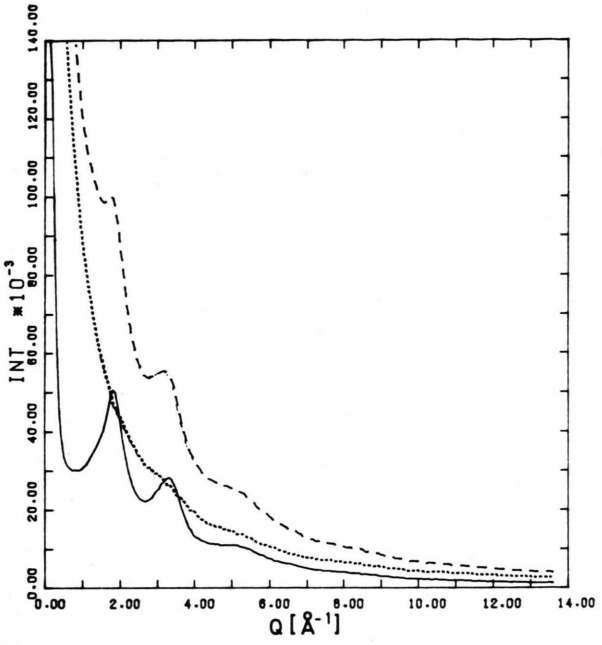

Fig. 4. Amorphous Germanium. Electron diffraction (50 kV). Comparison between an elastic and an inelastic measurement; ——— elastic measurement, ---- inelastic measurement, ... subtraction of both measurements.

that the plasmon scattering can be separated from the elastic part of the spectrum. All the other inelastic effects cannot be completely removed. These are: Phonon scattering which lies according to [11] at a few tenth eV and Compton scattering which lies at several eV and the contribution of which is according to [11] very small.

To demonstrate the function of the electrostatic filter, two measurements were performed, one with switched on filter ($U_{\mathrm{Bat}} = 0$ V) and the other with switched off filter. By subtracting the results of these measurements the inelastic background curve is obtained. The three curves are given in Figure 4. It is interesting to observe that the diffraction peaks are totally eliminated in the background curve. The background curve represents the inelastic part of the electron spectrum which is eliminated by the filter, that means, mainly the plasmon excitations.

The full line in Fig. 4, which represents the elastically scattered electrons, shows a very pronounced run.

To obtain insight into the influence of multiple scattering on the diffraction pattern, Germanium specimens with different thicknesses were examined. The preparation was done in a high vacuum evaporation apparatus with an oscillating quartz thickness measuring device. The diffraction patterns are compiled in Figures 5 a and 5 b. If the curves are normalized at their first maximum as done in these figures, the following observations can be made:

With increasing thickness up to 100 Å going to larger angles the intensity decreases very fast. For samples thicker than 100 Å this behaviour is reversed as can be seen from Fig. 5 b, where the decrease of intensity becomes smaller with increasing thickness.

In Fig. 6 a diffraction pattern is shown which was obtained with a very thin Ge-specimen. From the fact that it oscillates very well around f^2 we as-

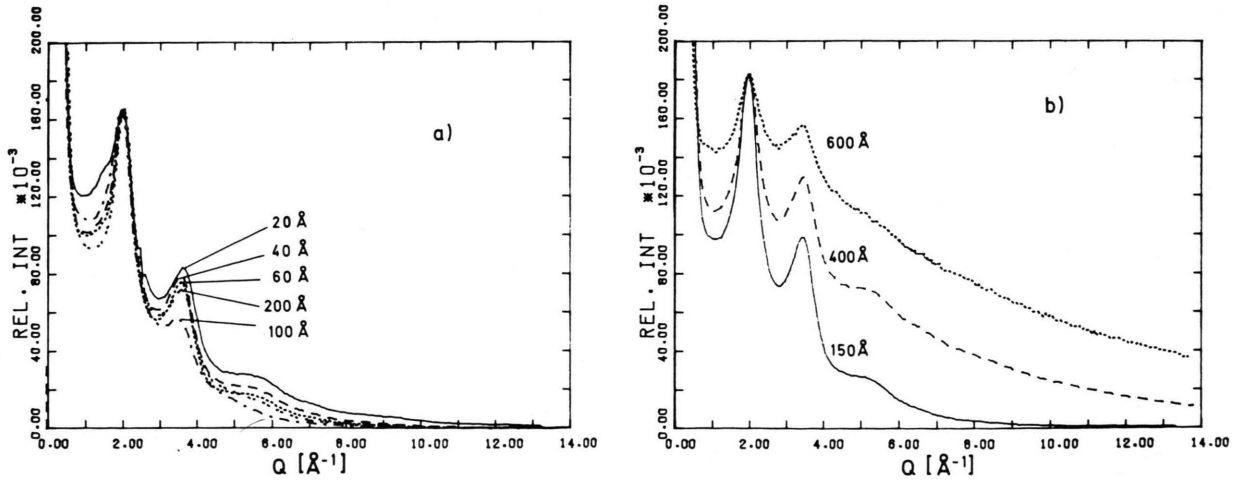

Fig. 5a. b. Amorphous Germanium. Electron diffraction (50 kV). Specimens with different thicknesses. Intensities normalized at the first maximum.

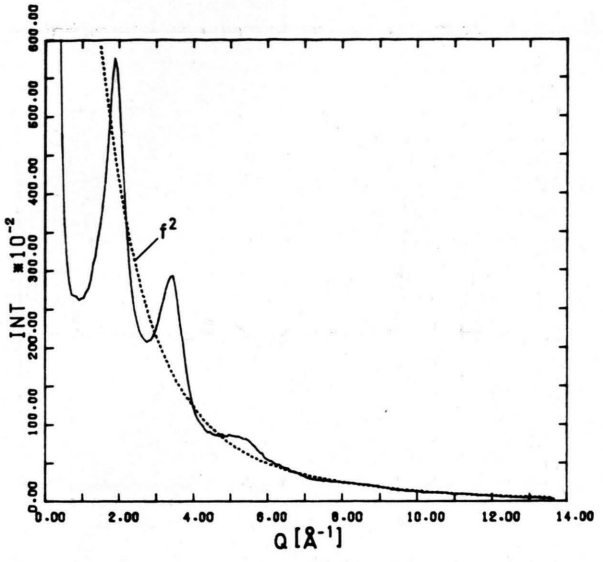

Fig. 6. Amorphous Germanium (20 Å). Electron diffraction (50 kV). Intensity curve.

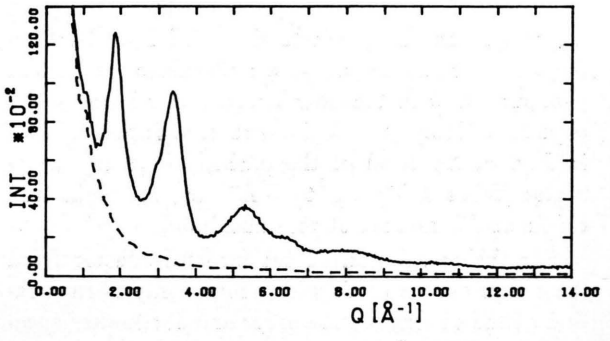

Fig. 7. Amorphous Germanium (5000 Å). X-Ray diffraction (Mo-Kα). Intensity curve. ——— Amorphous Germanium on substrate (mica 5 μm); ----- Substrate (mica 5 μm).

sume that the contributions from multiple scattering are very small. This diagram shall be compared with a corresponding diagram obtained using X-Rays. The latter was measured with a diffractometer (Type D 500; Siemens) using MoKα-radiation together with the filter-method according to Ross [12]. Figure 7 shows the intensity curve obtained with amorphous Germanium fixed on a substrate (mica foil 5 μm thick) and with the substrate alone.

Evaluation

Correction of the electron diffraction patterns obtained with the apparatus described above for multiple scattering was done according to the method given in [13]. This method was checked for the case of amorphous Germanium and then applied to amorphous $Mn_{73}Si_{27}$ [14]. Before describing the correction method it should be mentioned that the correction method as applied very often in the past, which is based on the background of a crystalline reference specimen [15] can be well applied for an inelastic background which contains only a small contribution of multiple scattering. However, for strong multiple scattering the method according to [15] should not be applied since the background produced by multiple scattering within a crystal in any case will not be identical with that produced within an amorphous specimen.

The correction method [13] can be described as follows: Starting from a thin slice of the specimen in which only single scattering occurs, the total scattering of the thick specimen is obtained as superposition of many thin films. From the mathematical point of view this corresponds to many integrals inserted into one another. These integrals can be reduced to a simple multiplication by a so called Hankel transformation, i. e. the presentation of the intensity curves in the complete orthogonal system of Bessel functions of zero'th order. The corresponding procedure can be sketched as follows:

i) Normalization of the intensity curve:

$$\int_0^\infty s\, I(s)\, \mathrm{d}s = 1 \tag{4}$$

with $s = 2\,\theta$. In an approximation s is calculated as

$$(\lambda/2\,\pi)\, Q\,.$$

ii) Hankel transformation:

$$f(l) = \int_0^\infty s\, I(s)\, \mathrm{J}_0(l\, s)\, \mathrm{d}s \tag{5}$$

with J_0 = Bessel functions of zero'th order. The intensity curve is represented in Hankel-space as $f(l)$.

iii) Reduction of the multiple scattered curve $f(l)$ into a scattering curve of first order $f_1(l)$:

$$f_1(l) = 1 + \ln\left(I/I_0 + \frac{1 - I/I_0}{f(l)}\right) \Big/ (-\ln I/I_0). \tag{6}$$

The multiple scattering parameter I/I_0 is the ratio of the transmitted intensity to the total intensity. Thereby only that intensity may be regarded which was elastically scattered out of the primary beam, i. e. an intensity which cannot be measured. There-

fore I/I_0 means a free parameter for the performance of the correction method for multiple scattering.

iv) Back-transformation:

$$I_1(s) = \int_0^\infty l f_1(l) J_0(l s) \, dl . \qquad (7)$$

The correction parameter I/I_0 has to be chosen in a way that the resulting corrected structure factor $S(Q)$ shows a run which oscillates properly around unity at higher Q-values. Figure 8 shows some results to demonstrate the effect of the multiple scattering correction procedure. The difference in the run between the solid and the dashed curves is caused by uncertainties in the choice of the parameter I/I_0. In the region of the fifth maximum ($Q \approx 11$ Å^{-1}) the structure factors run out of phase. For the 200 Å specimen the choice was $I/I_0 = 0.21$ and 0.15, respectively. For the 400 Å specimen (Fig. 5 a) I/I_0 was 0.06. The latter specimen yielded a rather uncertain result since this specimen is rather thick and therefore the degree of multiple scattering is rather high. Nevertheless the coincidence up to $Q = 5$ Å^{-1} is very good.

In Fig. 9 we present the I/af^2-curve obtained with the very thin Germanium-specimen from Fig. 6 once uncorrected (–) and once corrected (– – –). For $Q > 7$ Å^{-1} the dashed line shows an improved run compared to the solid line. Furthermore the maxima at lower Q-values are more pronounced with the corrected curve as was to be expected. Compared to the structure factors shown in Fig. 8, the level of the dashed curve in the Q-region from 1 Å^{-1} up to 5 Å^{-1} is too high. The origin of this fact is not yet understood.

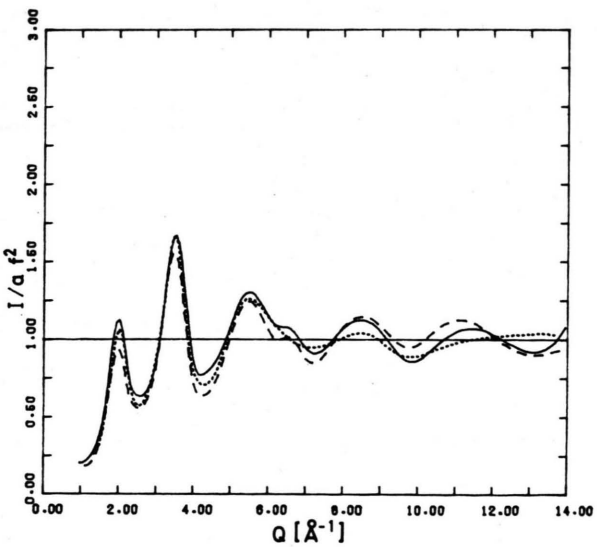

Fig. 8. Amorphous Germanium. Electron diffraction (50 kV). I/af^2-curves corrected for multiple scattering. ——— 200 Å $I/I_0 = 0.21$; – – – – – 200 Å $I/I_0 = 0.15$; ..... 400 Å $I/I_0 = 0.06$.

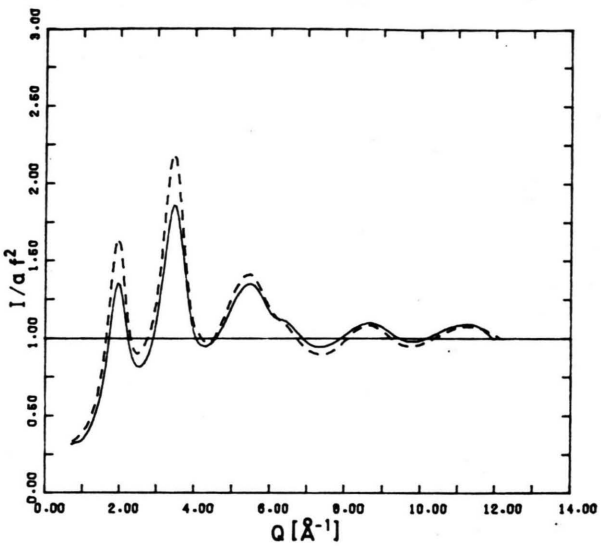

Fig. 9. Amorphous Germanium (20 Å). Electron diffraction (50 kV). I/af^2-curves. ——— without correction for multiple scattering; – – – – – with correction for multiple scattering ($I/I_0 = 0.7$).

For the calculation of the structure factor from the rough curves of thin specimens only normalization of the experimental curves and for thicker specimens in addition a correction for multiple scattering is necessary. There is no need for a correction for absorption since the scattering angles (max. 7°) are much smaller than in the X-Ray case and thus the path of all electrons, even when multiple scattered, has nearly the same length. The normalization of the scattering curves was done according to Krogh-Moe [16].

Having once evaluated the total structure factor the further evaluation procedure is the same as for X-ray or neutron experiments. The pair correlation function $G(r)$ is calculated from the structure factor according to (2). From the $A(r)$-function according to (3) we obtain by integration between the neighbouring minima around a maximum the corresponding coordination number. Figure 10 shows the pair correlation functions $G(r)$ for Germanium. The values for $G(r_1)$ and the coordination number

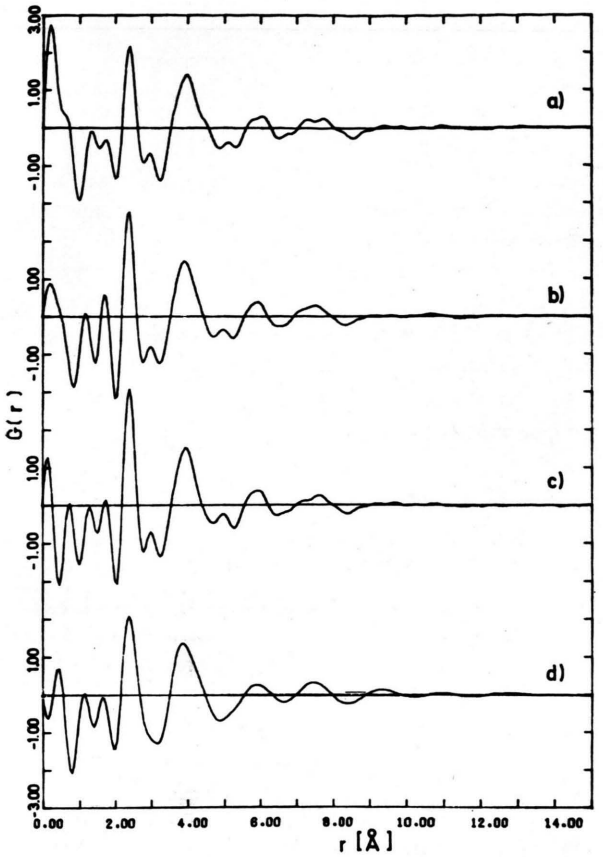

Fig. 10. Amorphous Germanium. Electron diffraction (50 kV). Pair correlation function $G(r)$. a) 20 Å without correction for multiple scattering; b) 200 Å $I/I_0 = 0.21$; c) 200 Å $I/I_0 = 0.15$; d) 400 Å $I/I_0 = 0.06$.

N_1 for the first coordination sphere are given in Table 1.

Table 1 also contains the corresponding figures from the X-Ray experiment, which was evaluated according to Ref. [17] and which yielded after correction for absorption, polarization, and Compton scattering the structure factor shown in Figure 11. In spite of the fact that with an element no differences are to be expected between the structure

Table 1. Amorphous Ge. Electron diffraction (50 kV): $G(r_1)$ and N_1 (* X-Ray diffration).

Thickness [Å]	I/I_0	$G(r_1)$	N_1
20	—	2.15	3.7
200	0.21	2.78	3.8
200	0.15	3.07	4.1
400	0.06	2.10	4.3
5000*	—	4.81	4.3

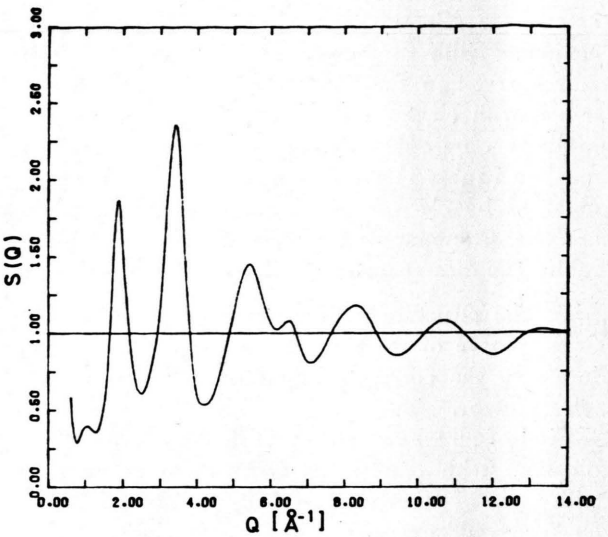

Fig. 11. Amorphous Germanium (5000 Å). X-Ray diffraction (Mo-Kα). Structure factor $S(Q)$.

factors obtained with different kinds of radiation, the X-Ray (Fig. 11) and electron (Fig. 8) structure factors differ. The X-Ray structure factor oscillates around unity by a factor of two more strongly than the electron structure factor. The oscillation, however, is more attenuated for large Q's. The line width of the maxima is nearly the same. The splitting of the third maximum is more pronounced in the X-Ray curve. From the X-Ray structure factor of Fig. 11 the pair correlation function $G(r)$ of Fig. 12 was calculated.

Discussion

In this section the pair correlation functions $G(r)$ and the coordination numbers N_1 obtained for

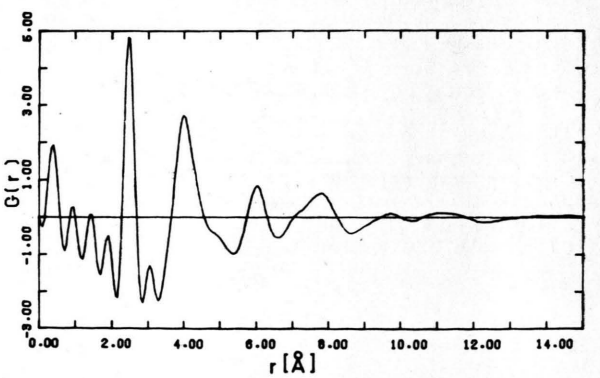

Fig. 12. Amorphous Germanium (5000 Å). X-Ray diffraction (Mo-Kα). Pair correlation function $G(r)$.

amorphous Germanium will be discussed and compared with the results of other workers. The pair correlation functions $G(r)$ from Fig. 10 obtained with electrons show pronounced differences to those obtained with X-Rays (Figure 12). All maxima (Table 1) are less pronounced in the curve obtained by electron diffraction. Also the minima are less pronounced. The line widths are comparable. The discrepancies may have different origins:

i) The structure factor calculated from the intensity curve of the diffracted electrons and therefore also the corresponding $G(r)$ contains a systematic error.

First of all we can state that the structure factors obtained with amorphous Germanium agree well with those of other workers [18, 19]. In [18] also an "elastical" experiment (energy resolution 3 eV) was performed, whereas in [19] the inelastically scattered background was measured with a crystalline Germanium specimen and fitted according to [15].

Furthermore we can state that the $G(r)$-curves obtained with amorphous Gallium once with X-Rays and once with electrons [20, 21] show the same discrepancies though the authors didn't mention them.

Concerning systematic errors which in principle must be considered for the explanation of the rather large discrepancy in the Germanium structure factor as obtained with X-Rays and electrons, respectively we can state the following on behalf of our experience: The X-Ray method yields compared to the neutron method identical results (see for example the element Lithium [22]) and therefore the discrepancies must have their origin in the electron diffraction method. In this connection we exclude changes of the specimen by electron impact and the influence of the specimen thickness (compare Figure 8). A certain contribution to the discrepancy perhaps may be caused by remaining uncertainties in performing the correction for multiple scattering and for inelastic scattering.

ii) The discrepancies between the X-Ray and the electron curves are caused by the different scattering process:

Most probably these discrepancies are of more fundamental nature and can be reduced to the very strong interaction of the electrons with the specimen. This means that the aspect of dynamical scattering even in non crystalline substances should be taken into consideration as already was proposed in an earlier paper [23].

Acknowledgements

Thanks are due to the Deutsche Forschungsgemeinschaft, Bad Godesberg, for financial support of this work and to Prof. Dr. C. Burggraf, University of Strasbourg, for the construction of the electrostatic filter and the readiness to help in many points with his advice.

[1] C. Grigson, in: Advances in Electronics and Electron Physics, Academic Press, London 1968.
[2] R. A. Bonham and L. Fink, High Energy Electron Scattering, Van Nostrand, Amsterdam 1974.
[3] S. H. Bauer, Electron diffraction techniques for the study of amorphous systems, in: Non Crystalline Solids, ed. by Frechette, John Wiley, New York 1960.
[4] D. Geissler and K. H. Gaukler, Optik **38**, 406 (1973).
[5] C. Bovier, These D'etat, Strasbourg 1974.
[6] J. F. Graczyk and S. C. Moss, Rev. Sci. Instrum. **40**, 124 (1969).
[7] C. Burggraf, private communication.
[8] C. D. Bunting, Proc. 25th Anniversary Meeting of Emag. Inst. Phys. 1971.
[9] C. Gerthsen and H. O. Kneser, Physik, Springer-Verlag, Berlin 1971, p. 301.
[10] H. Grabe, Dissertation, Kaiserslautern 1979.
[11] H. Raether, Springer Tracts in Modern Physics **38**, 84 (1965).
[12] H. Küstner, Z. Physik **70**, 468 (1931).
[13] J. Gjonnes, Acta Cryst. **12**, 976 (1959).
[14] F. Paasche, H. Olbrich, G. Rainer-Harbach, P. Lamparter, and S. Steeb, Z. Naturforsch. **37a** (1982), in press.
[15] S. Steeb, Dissertation, Stuttgart 1958.
[16] J. Krogh-Moe, Acta Cryst. **9**, 951 (1956).
[17] J. P. Gabathuler, Dissertation, Stuttgart 1978.
[18] J. F. Graczyk and P. Chaudhari, I + II Phys. Stat. Sol. **58b**, 163 (1973).
[19] M. Gandais, M. L. Theye, S. Fisson, and J. Boissonade, Phys. Stat. Sol. **58b**. 601 (1973).
[20] A. Bererhi, L. Bosiv, and R. Cortes, J. Non-Cryst. Sol. **30**, 253 (1979).
[21] S. Fujime, Jap. J. Appl. Phys. **5**, 764 (1966).
[22] H. Olbrich, Dissertation, Stuttgart 1982.
[23] J. M. Cowley, Acta Cryst. **A24**, 329 (1968).